Check for updates

Original research article

Journal of Vibration and Control
2026, Vol. 0(0) 1–15
© The Author(s) 2026
Article reuse guidelines:
sagepub.com/journals-permissions
DOI: 10.1177/10775463261428650
journals.sagepub.com/home/jvc
Sage

Vehicle response to hydroplaning: Evaluation of driver reaction using a dynamic driver simulator

Edoardo Montini[1], Edoardo Sabbioni[1] and Stefano Melzi[1]

Abstract

Hydroplaning poses a significant risk to road safety, as a water wedge between the tires and the road reduces the vehicle's responsiveness to driver inputs. This phenomenon is influenced by factors such as vehicle speed, water depth, and tire wear, directly impacting parameters like cornering stiffness, relaxation length, and friction coefficient. This study evaluates a control logic designed to assist drivers during hydroplaning. A novel tire model was developed and integrated into a 14-degree-of-freedom vehicle model to simulate hydroplaning effects, while an Advanced Driver-Assistance System (ADAS) was designed to enhance vehicle control. A dynamic driving simulator was used to test driver interactions with the proposed control system and assess its effectiveness. The ADAS was evaluated in double-lane-change and high-speed turn scenarios, where drivers of varying experience levels were asked to complete the maneuver at different speeds, both with and without the control system's assistance. The control strategy helped the drivers to complete the maneuvers, reducing their effort on the steering wheel. In conclusion, this study provided valuable insights into how everyday drivers manage hydroplaning, highlighting ADAS's potential to improve vehicle control and safety in such conditions.

Keywords

ADAS system, driving simulator, hydroplaning, scenario, tire model

Received: 1 February 2025; accepted: 7 February 2026

Introduction

Hydroplaning is a critical factor in road safety, significantly increasing the risk of accidents under wet conditions. Statistics show that 10% of fatal crashes occur in adverse weather, with 7% on wet roads and 3% on icy or snow-covered surfaces (World Health Organization, 2019). Hydroplaning (Albert, 1968) occurs when a water layer separates the tires from the road, rendering braking and steering ineffective and creating a highly hazardous situation. Its risk depends on factors such as speed, water depth, and tire design (Raste and Frerichs, 2016), particularly the tread's ability to drain water. For a given water depth and tread design, speed is the key variable. The critical hydroplaning speed is the point at which the tire loses all the contact with the road, compromising stability and directionality. This loss of control, as highlighted by Malenska et al. (2021), severely limits the tire's responsiveness to driver inputs, increasing the likelihood of accidents, while Fwa et al. (2009) investigates the relationship between groove pattern and hydroplaning speed. Moreover, Metz (2012) and Metz (2014) simulated the hydroplaning development during transient maneuver, while Metz et al. (2006) investigated the real axle behaviour during straght motion.

Given the hazardous nature of hydroplaning, many studies have sought to mitigate its effects. Hartman et al. (2019) developed a control system using a simplified vehicle model to simulate hydroplaning, though it did not account for the forces on the front tires during the phenomenon. Other studies, such as Jindrich et al. (2019) and Blandina et al. (2020), proposed using air streams to spray water away from the front tires in order to reduce the risk of hydroplaning. Detecting the onset of hydroplaning is crucial for activating corrective systems. Niskanen et al. (2015) proposed various methods and devices for detecting hydroplaning, while Wong (2001) developed a system aimed at

[1]Mechanical department, Politecnico di Milano, Milano, Italy

Corresponding author:
Edoardo Montini, Mechanical department, Politecnico di Milano, Via LaMasa, 1, Milano, 20156, Italy.
Email: edoardo.montini@polimi.it

recognizing hydroplaning conditions at the vehicle level, a potentially important tool for preventing accidents.

The aim of this paper is the development of an Advanced Driver Assistance System (ADAS) leveraging smart tire technology for hydroplaning detection. When hydroplaning is detected by the smart tires, the proposed controller assists the driver by reducing vehicle speed and generating a corrective yaw moment through rear-wheel torque vectoring. The controller was developed and tuned using numerical simulations and subsequently validated in a dynamic driving simulator to assess interactions with real drivers and to evaluate driver feedback.

A key component of the simulation environment is a tire model capable of accurately reproducing vehicle and driver feedback under hydroplaning conditions while remaining suitable for real-time execution.

In the scientific literature (Aboeòsaoud et al., 2025; Yu et al., 2026; Zhong et al., 2025), hydroplaning is typically simulated using high-fidelity numerical approaches such as the Material Point Method (MPM) and the Finite Element Method (FEM). Although these methods provide highly accurate results and are widely used for tire tread pattern design, their computational cost makes them unsuitable for real-time applications such as the one addressed in this paper. To overcome this limitation, the present work introduces a real-time-capable empirical tire model based on Pacejka's Magic Formula (Pacejka, 2006). The model is enhanced through scaling factors applied to the peak friction coefficient, cornering stiffness, longitudinal stiffness, and relaxation lengths, enabling the reproduction of hydroplaning dynamics across a range of maneuvers, including frequency sweep steering inputs and double lane-change tests.

This system will be tested in a dynamic driving simulator Gobbi et al., (2022) to assess its effectiveness in real-time under hazardous conditions, particularly for less experienced drivers. In addition to evaluating the performance of the ADAS, the study will analyze both objective measures—such as driving performance—and subjective factors, such as driver feedback and trust in the system, to provide a comprehensive understanding of its potential impact.

Tire model development

A novel tire model was developed, building on the well-known Pacejka's MF-Tire model (Pacejka, 2006). The original Pacejka model, widely used for describing tire-road adhesion forces, can be extended to simulate vehicle behavior during hydroplaning by introducing specific scaling factors, derived from experimental studies under hydroplaning conditions. These modifications adjust the model's parameters based on key variables, such as vehicle speed, water depth, and tire and road surface characteristics. These changes aim to represent the loss of adhesion due to water more accurately, improving the prediction of traction, braking, and steering forces under hydroplaning conditions (Wong, 2001).

In practice, this scaling process involves altering parameters like the maximum adhesion coefficient, the adhesion force's peak position, and the adhesion curves' shape. The adjustments reflect the significant loss of grip that occurs when water causes separation between the tire and the road surface. Such modifications are crucial for accurate vehicle simulation during critical phases like hydroplaning, providing valuable data for the design of advanced control systems, such as Anti-lock Braking Systems (ABS) and Electronic Stability Control (ESC).

MF-tire model for hydroplaning condition

The model requires input parameters such as camber, slip angle (α), longitudinal slip (κ), and relaxation length (λ), and it outputs the forces the tire exchanges with the ground. The MF-Tire model relies on simple analytical expressions for the calculation of both lateral (F_y) and longitudinal (F_x) forces

$$\begin{cases} F_y(\sigma) = D_y\, sin\big(C_y\, atan\big(B_y\sigma - E_y\big(B_y\sigma - atan\big(B_y\sigma\big)\big)\big)\big) \\ F_x(\sigma) = D_X\, sin\big(\, C_x\, atan\big(B_x\sigma - E_x\,\big(B_x\sigma - atan\big(B_x\sigma\big)\big)\big)\big) \end{cases} \tag{1}$$

in the previous equations, B represents the stiffness factor, C the shape factor, D the peak force defined as $D = s_a{*}\mu{*}F_z$, where μ is the maximum friction coefficient between the tire and the road, F_z is the tire vertical load and s_a is the friction coefficient scaling factor, and E the curvature factor. Therefore, the cornering and longitudinal stiffnesses can be obtained as

$$\begin{cases} K_y = s_y{*}B_y \cdot C_y \cdot D_y \\ K_x = s_x{*}B_x \cdot C_x \cdot D_x \end{cases} \tag{2}$$

s_x and s_y refer to the scaling factors associated to the longitudinal and lateral stiffness.

Furthermore, the MF-Tire model also accounts for combined slip conditions, where both longitudinal and lateral forces are developed simultaneously (equation (3)). The interaction between these forces is governed by the slip ratio and slip angle, resulting in a combined force representation crucial for accurate vehicle dynamics modeling

$$\sigma_x = \frac{\kappa}{1+\kappa};\ \sigma_y = \frac{tan(\alpha)}{1+\kappa};\ \sigma = \begin{Bmatrix} \sigma_x \\ \sigma_y \end{Bmatrix} \tag{3}$$

The transient behavior of the tire is reproduced through a 1st order differential model; lateral and longitudinal forces are delayed by the time constants $\frac{v}{\lambda_y{*}s_y^{rel}}$ and $\frac{v}{\lambda_x{*}s_x^{rel}}$

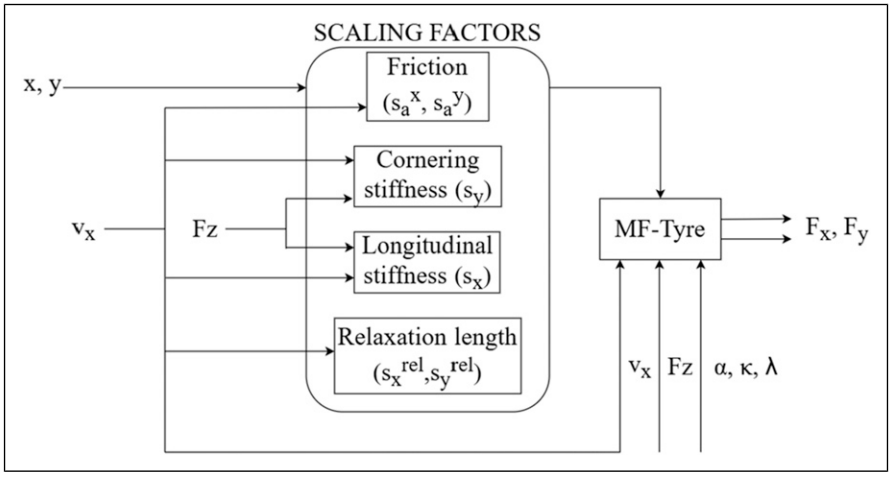

Figure 1. Scheme of the MF-tire model accounting for hydroplaning scaling factors.

$$\begin{cases} \frac{\lambda_y * s_y^{rel}}{v}\dot{F}_y + F_y = F_{y,ss} \\ \frac{\lambda_x * s_x^{rel}}{v}\dot{F}_x + F_x = F_{x,ss} \end{cases} \quad (4)$$

v represents the longitudinal speed of the wheel center, while λ_y and λ_x refer to the relaxation lengths in the lateral and longitudinal directions, respectively, and s_y^{rel} and s_x^{rel} their relaxation length scaling factor.

A scheme of the model can be checked in the following figure (Figure 1).

Scaling factors are implemented as lookup tables, with the appropriate scaling determined based on the vehicle's speed input. For practical implementation, hydroplaning is defined at a specific spatial position. Consequently, the scaling factors must be activated when the vehicle's position coincides with the defined hydroplaning location.

Physical explanation of hydroplaning and hydroplaning speed

Hydroplaning occurs when a wedge of water lifts the tire's contact patch off the ground. This phenomenon includes partial hydroplaning, where only the front portion of the contact patch becomes detached, and full hydroplaning, where the entire contact patch is lifted, virtually rendering the tire unable to transmit forces to the ground. This second condition is much more dangerous than the first one, thus it is possible to define the hydroplaning speed as the speed above which full hydroplaning occurs. It is primarily influenced by factors such as tread pattern, tread wear, tire width, and water film thickness. Figure 2, taken from Raste (2016), illustrates the impact of tread depth (PT) and water thickness (WT) on hydroplaning speed, highlighting the direct relationship between the tread depth-to-water thickness ratio and hydroplaning risk: a higher ratio corresponds to a lower risk.

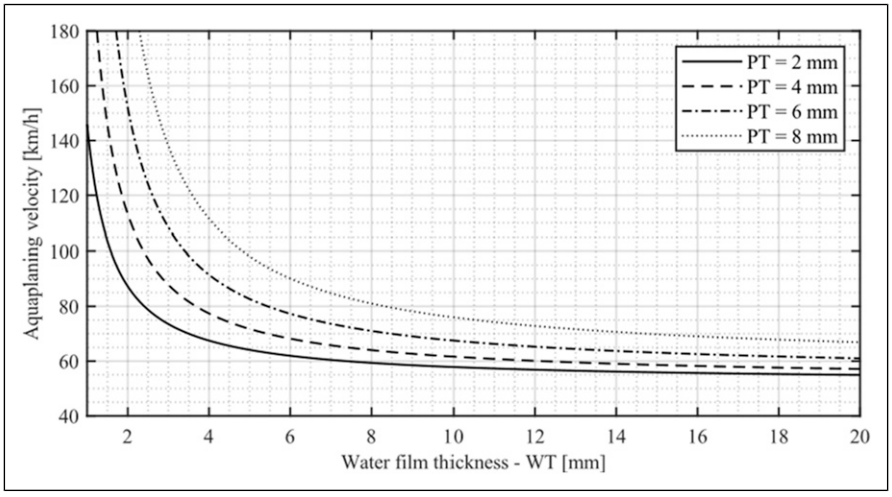

Figure 2. Hydroplaning speed versus water film thickness WT for different tread depths (Raste et al., 2016).

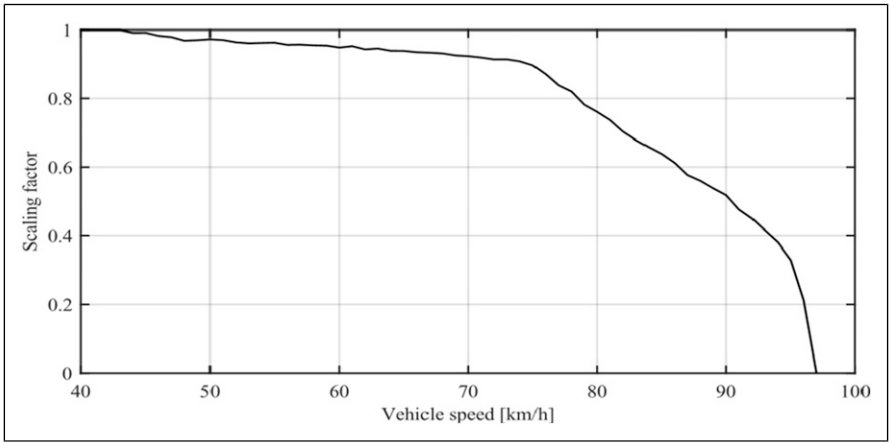

Figure 3. Scaling factor of friction coefficient Fichtinger (2021).

Furthermore, hydroplaning has been shown to predominantly affect the friction coefficient, relaxation length, and cornering stiffness, as evidenced by studies in Sbrosi (2012) and Fichtinger (2021). Since relaxation length and cornering stiffness are directly linked to tire type, the analysis focuses on a city car commercial tire. Arosio (2005) and Braghin (2006) confirm that the type of tire minimally influences the scaling factor for the friction coefficient.

Most important parameters and scaling factors

Several studies have explored how hydroplaning affects key vehicle parameters. For example, Sbrosi (2012) and Fichtinger (2021) focused on the impact of hydroplaning on tire cornering stiffness, relaxation length, and friction coefficient. Others, such as Mounce (2025) and Kienle (2020), have examined how road texture

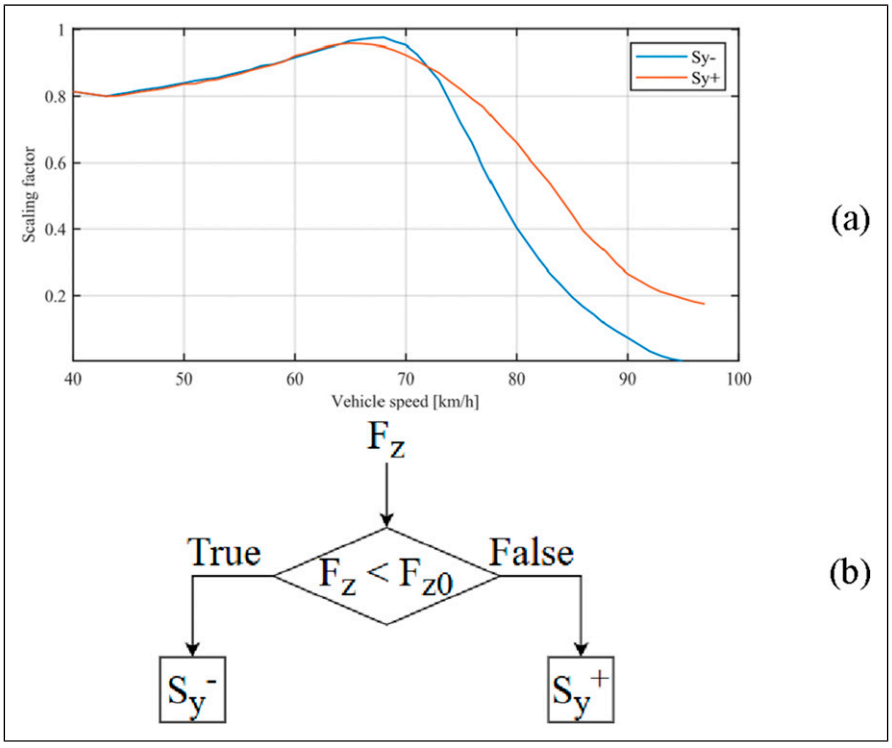

Figure 4. Scaling factor of cornering stiffness for positive and negative load transfer (Sbrosi et al., 2012) (a). Model logic to select the right scaling factor (b).

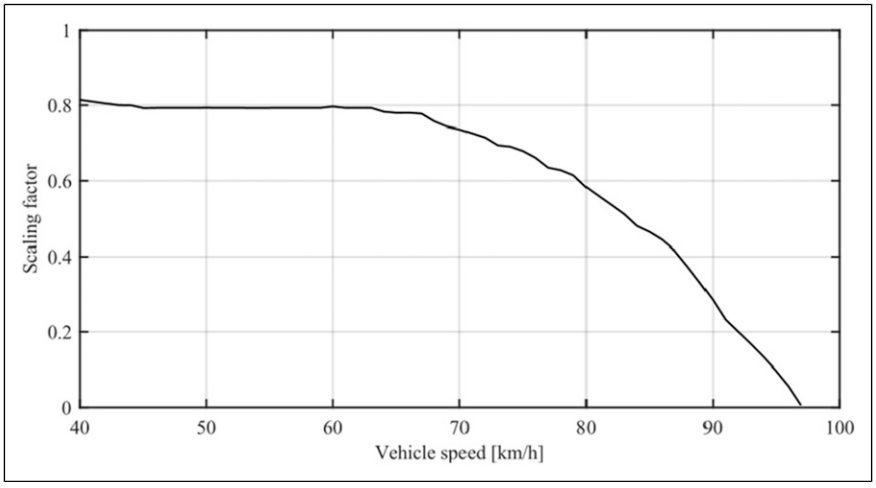

Figure 5. Longitudinal stiffness scaling factor (Fichtinger et al., 2021).

influences the onset and severity of hydroplaning. The design of the tire tread plays a crucial role as well, with Bielse et al. (2022) analyzing how tread design affects the maximum water flow a tire can handle, and Fwa et al., 2009 exploring how groove patterns impact the critical speed at which hydroplaning occurs. Further research by Cerezo (2010) and Metz (2011) confirmed that when the front tires experience hydroplaning, the rear tires can still generate some force, a phenomenon known as the cleaning effect, where the rear tires help clear water from the front tires, slightly reducing the effects of hydroplaning.

Friction coefficient

The friction coefficient between tire and road is a key parameter which determines the limit of the force transmittable to the ground. It affects the D parameter proportionally, raising the peak of the tire characteristic curve. Of course, traveling on wet roads causes a drop in the friction potential, especially during a hydroplaning event. In order to consider this phenomenon, the scaling factor presented in Figure 3 has been introduced in the model.

This relation between friction potential and vehicle speed in hydroplaning conditions has been obtained from Fichtinger (2021). Of course, the values μ obtained are referred to a certain tire model with a given vertical load. However, in this application, the shape of the scaling factors curve obtained is assumed valid for whichever tire model. During the simulations, vertical load variations are included thanks to a load transfer model directly implemented in the 14 dof vehicle model.

Cornering and longitudinal stiffness

In this model, a crucial role is played by the scaling factors that reduce the value of the cornering stiffness. Starting from the outcomes obtained in Sbrosi (2012), a

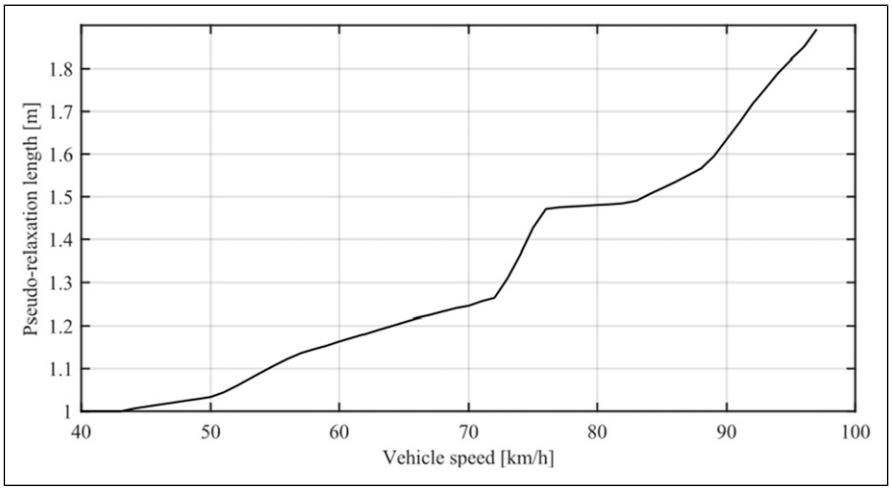

Figure 6. Pseudo-relaxation length obtained by Sbrosi (2012).

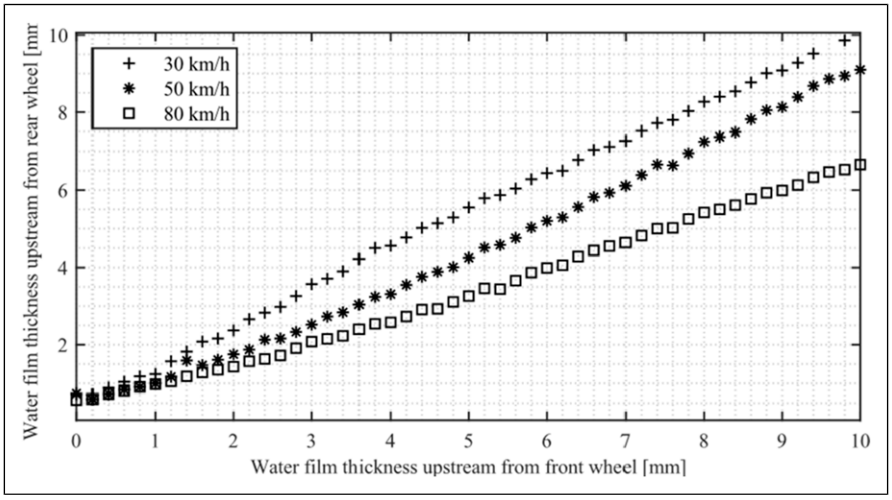

Figure 7. Relationship water film thickness front versus rear (Cerezo et al., 2011).

set of values included between 0 and 1 was derived as a function of vehicle speed. As can be noted from Figure 4(a), two different curves are necessary for the cornering stiffness scaling factor. This is due to the lateral load transfer occurring on the vehicle during turning maneuvers. When this leads to an increment of the vertical load on the tire, the red curve has to be considered. Otherwise, the blue one must be taken into account.

Figure 4(b) illustrates the selection of the appropriate curves for a tire, indicating the correct scaling factor to be applied based on the tire's actual load.

Figure 5 shows the longitudinal stiffness scaling factor. Changes in slip stiffness relative to vehicle speed provide an early indication of potential hydroplaning risk. Indeed, comparing the Figure 5 with respect to Figure 3, associated to the reduction of the friction coefficient, longitudinal stiffness drop appears at lower speeds.

Relaxation length

Tire relaxation length allows to consider the delay between the steady-state force suggested by Pacejka and the transient one. What is observed experimentally is that the tire relaxation length λ is very influenced by the conditions of the ground the vehicle is running on. In Sbrosi (2012), the behavior of λ as a function of the vehicle speed is investigated.

As it is possible to notice in Figure 6, values of λ tend to strongly increase as the vehicle approaches hydroplaning speeds: at 90 km/h, the relaxation length is nearly doubled with respect to the nominal one. This indicates that at velocities close to hydroplaning ones, not only is the tire less capable of generating traction and cornering forces, but in order to generate those forces, a strong time delay is needed.

Extension of the scaling factors to different water film thickness

When the hydroplaning speed is exceeded, the water layer lifts the tire, eliminating road contact. Due to limited experimental data, the tire is assumed to have a maximum volumetric drainage capacity, expressed as

$$V = A * t * v \tag{5}$$

where V is the volumetric flow rate, A is the frontal area of the tire, t is the water film thickness, v is the vehicle speed. Literature provides scaling factors evolution with speed (Fichtinger et al., 2021; Sbrosi et al., 2012) at a single water film thickness, and the evolution of the hydroplaning speed as a function of water film thickness and tread pattern (Raste et al., 2016). Therefore, to extend the available scaling factor curves to different water film thicknesses, the maximum volumetric flow rate of the tire must be known. This can be derived from Sbrosi (2012), using the testing speed, film thickness, and tire geometry. For a new water film thickness t_{New}, the hydroplaning speed is computed a

$$v_{Hydro} = \frac{V}{A * t_{New}} \tag{6}$$

Below this speed, the tire remains in contact with the ground, and scaling factors are unchanged with respect to Figures 3–6. For speeds above $v_{Hydro,New}$, grip decreases as scaling factors drop. To account for this across multiple water thicknesses, an equivalent speed is introduced to map the new condition onto the reference curves

$$v_{equiv} = \frac{v}{v_{Hydro,New}} * v_{Hydro,ref} \tag{7}$$

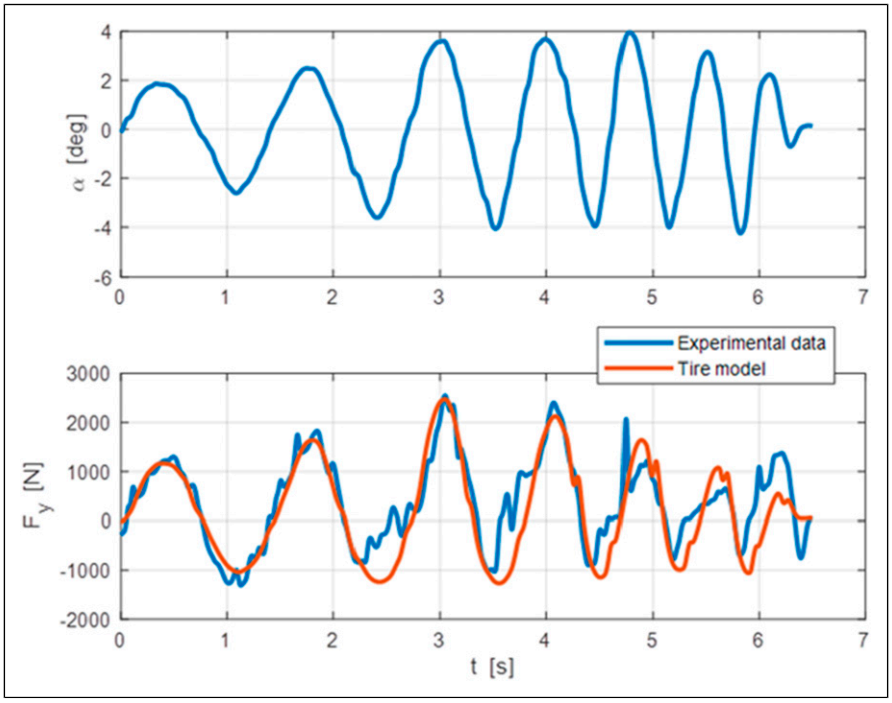

Figure 8. Model validation with respect to experimental data available in Sbrosi (2012).

where:

- $v_{Hydro,New}$ is the hydroplaning speed for the new water thickness
- $v_{Hydro,ref}$ is the hydroplaning speed under reference condition (Sbrosi et al., 2012)
- v is the speed at the new water thickness
- v_{equiv} is the equivalent speed used to retrieve scaling factors from reference curves.

This approach ensures consistency when extrapolating scaling factors beyond the original test conditions.

Rear tires: Cleaning effect

So far, the discussion primarily addresses the behavior of a single tire encountering a specific water layer depth at a given speed. This approach is especially relevant for the front tires. However, numerous studies have examined the "cleaning effect," wherein the rear tires benefit from the front tires' displacement of water from the road surface (Metz et al., 2011). This effect, incorporated into the present model, results in an elevated critical hydroplaning speed for the rear axle. As a result, the rear tires can often maintain road contact even when the front tires are fully hydroplaning. This variation in water depth between the front and rear wheels occurs because the front tires remove a portion of the water film, and the interval before the rear tires encounter the same area is typically insufficient for the water layer to re-form fully. A key factor here is the "recovering speed" (*Vr*), defined as the speed at which the water film begins to regenerate between the front and rear tires. By analyzing this speed in relation to water film depth, it is possible to model the relationship between the water film depths experienced by the front and rear tires (Cerezo et al., 2010), as illustrated in Figure 7.

According to Cerezo (2011), for speed above 80 km/h, the water-film thickness can decrease until 30% between the front and the rear wheels. This model provides insight into the differential conditions affecting front and rear tires during hydroplaning, thereby improving predictions of vehicle stability in wet conditions.

In conclusion, critical hydroplaning speed on the rear tires can be estimated to be 35 km/h above the front one. Since in this work, highway running condition will be analyzed, it is possible to state that rear tires are running on partial dry asphalt, keeping the ability to respond to driver inputs.

Model validation

To verify that the proposed tire model is able to faithfully reproduce a hydroplaning condition, it is necessary to conduct an appropriate model validation. To do so, experimental data obtained from Sbrosi (2012) have been given as input to the model. The maneuver consists in a swept sine steer test with steering frequency between 0.5 Hz and 2.5 Hz, on a special straight track filled with 8-mm-deep water layer, and a vehicle speed of 85 km/h. Figure 8 reports the test slip angle given as input to the model and the

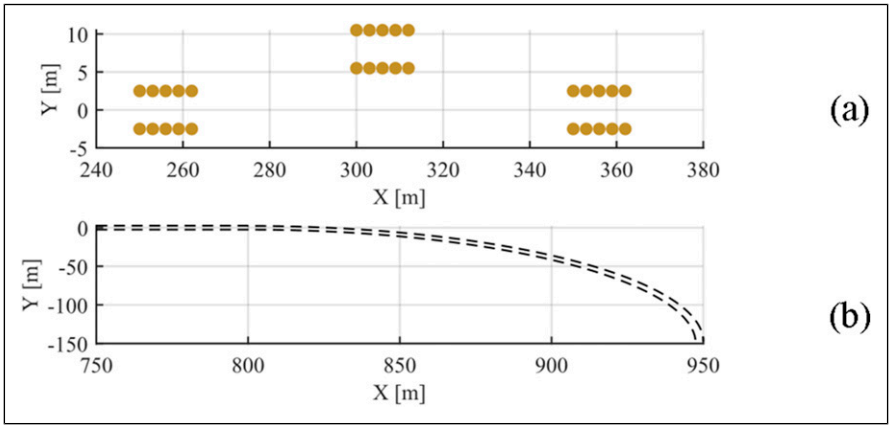

Figure 9. Selected maneuvers for simulations: Double lane change (DLC) (a), constant radius turn (b).

comparison between the experimental lateral forces acquired through smart tires and the numerical lateral forces computed by the simulation. The model reproduces the experimentally observed asymmetry in the tire response to a sine-sweep input and reasonably captures the frequency-dependent reduction in cornering force.

In general, the force asymmetry due to load shift during turning is much more pronounced compared to dry road conditions, due to the hydrodynamic interaction between tire and water that characterizes the hydroplaning phenomenon. This effect is introduced by the scaling factor on the normalized cornering stiffness presented in Figure 4. Another noteworthy effect is that of relaxation length, which significantly delays the development of the lateral force: as can be appreciated, with an increase in the sweep frequency, a significant decrease in lateral force is observed, even at relatively low frequencies like 2.5 Hz.

ADAS for hydroplaning prevention

To mitigate the effects of hydroplaning, this paper proposes an Advanced Driver Assistance System (ADAS) that leverages smart tires capable of detecting hydroplaning risk in real time (Niskanen et al., 2015; Niskanen et al., 2014; Niskanen et al., 2015). When hydroplaning is detected, the developed ADAS assists the driver by reducing vehicle speed and applying rear-wheel torque vectoring. The latter is particularly effective because the rear tires operate on a road surface partially cleared of water by the front tires.

The ADAS was developed through offline numerical simulations using a 14-degree-of-freedom vehicle model implemented in the VI-CarRealTime (VI-CRT) environment and equipped with the hydroplaning tire model previously described. The proposed real-time tire model is employed to simulate the onset of hydroplaning and to estimate the available tire–road friction under varying water-film conditions. By providing a physics-based representation of tire–road interaction during hydroplaning, the model enables the simulation of a wide range of driving manoeuvres, including double lane-change tests.

Finally, the developed ADAS was evaluated through driver-in-the-loop simulations conducted on the Politecnico di Milano dynamic driving simulator (DriSMi), with the aim of assessing driver feedback.

ADAS strategy

The ADAS control strategy is activated by smart tires that are the responsible in detecting the phenomenon (Niskanen et al., 2014; Niskanen et al., 2015). The goals of the logic are essentially two:

- First, to reduce the speed of the vehicle below the hydroplaning speed, in order to ensure its safety and stability.
- Second, to create a yawing moment that allows the driver to complete the maneuver when the vehicle is facing a maneuver that involves strong lateral dynamics.

As already explained, when hydroplaning occurs, rear tires are the only one still in contact with the ground, thanks to the cleaning effect. Thus, firstly the logic cuts the engine power, and disengages the brake pedal to prevent destabilizing forces, then it applies braking torque to the rear axle depending on the steering wheel angle (SWA) asked by the driver. If $-5 < SWA < 5$, the braking torque is equally distributed on the left and right wheel, thus no torque vectoring is applied. Instead, if $|SWA| > 5$, the yaw rate $\dot{\psi}$ defines the direction of the turn. The logic considers if the vehicle is understeering or oversteering, examining the error between the vehicle's yaw rate and reference yaw rate ($\dot{\psi}_{ref}$). This latter defines the yaw rate that the vehicle should maintain during a maneuver according to driver SWA inputs and

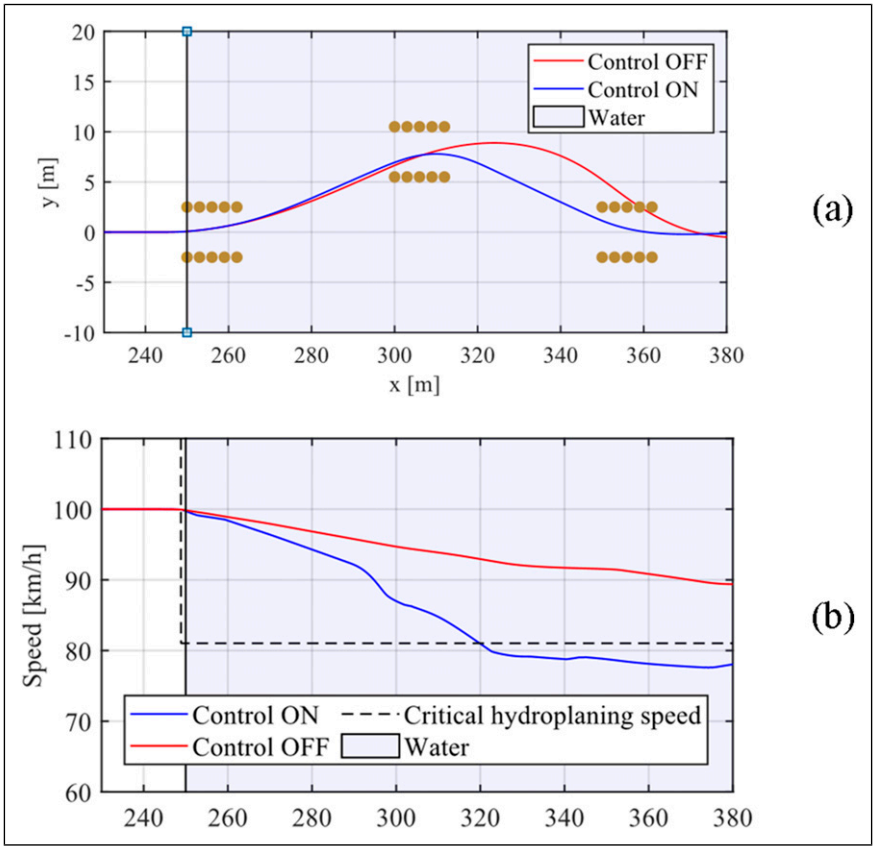

Figure 10. Offline simulation comparison between the activated and deactivated logic in terms of trajectories (a), the vehicle speed variation during the maneuver (b).

vehicle features. It is calculated according to equation (5), where v is the vehicle speed, SWA the steering wheel angle input, l the vehicle wheelbase, and $Kdes$ the desired understeering coefficient for the vehicle

$$\dot{\psi_{ref}} = \frac{v*SWA}{l(1 + K_{des}v^2)} \tag{8}$$

The error between yaw rate and reference yaw rate is reported as follows

$$\Delta\dot{\psi} = \dot{\psi_{ref}} - \dot{\psi} \tag{9}$$

If the vehicle's yaw rate is smaller (higher) in magnitude than the reference yaw rate, it means that the car is turning less than desired by the driver, thus is understeering (oversteering). In this case, the inner (outer) wheel of the curve will be braked more to create a yawing moment that tightens (widens) the trajectory.

Proposed maneuvers

Hydroplaning becomes increasingly hazardous as vehicle speed and water levels rise, posing significant risks under typical highway conditions. Prior studies have introduced methodologies for assessing a driver's ability to maintain control through performance metrics such as steering rate and angular acceleration (Erseus et al., 2013), while others have examined the effects of simulator fidelity and scenario complexity on driver workload using physiological and self-reported measures, including heart rate, pupil dilation, and cognitive stress levels (Mueller et al., 2014). Building on these findings, this study focuses on high-risk highway scenarios, emphasizing key maneuvers used to evaluate vehicle handling and driver control. One such maneuver is the double-lane-change (DLC) test (Figure 9(a)), which assesses a vehicle's ability to evade sudden obstacles by executing two successive lane changes. Commonly performed on highways for overtaking or obstacle avoidance, the DLC imposes significant lateral forces on the vehicle (Jalali et al., 2013). Although its dimensions are defined in ISO 3888-2, modifications were made to accommodate drivers with varying skill levels. As illustrated, the first lane change occurs between 250 m and 300 m, followed by the second between 300 m and 350 m, with a return to the original lane beyond 350 m. Another key maneuver is the constant-radius high-speed turn (Figure 9(b)), which, with its 150-m radius, evaluates vehicle stability under sustained lateral acceleration.

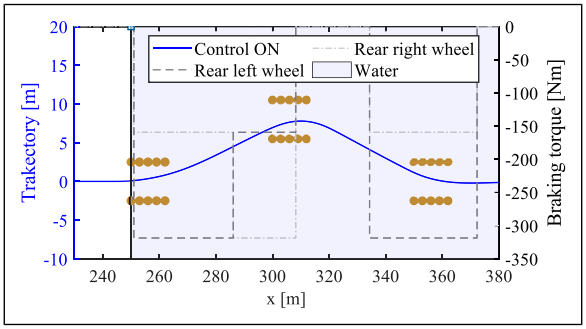

Figure 11. ADAS control logic working principle.

Offline simulation

Before conducting tests on the driving simulator, offline simulations were carried out to evaluate the performance of both the control logic and the tire model. Offline simulation serves as a crucial step for tuning the control parameters and optimizing the strategy under ideal driver conditions. To this end, a driver model was implemented, where a PD controller governed the steering input and a PID controller managed throttle and braking actions.

As an illustrative case, the validity of the tire model was evaluated through a Double Lane Change (DLC) maneuver at a speed of 100 km/h with a water film thickness of 5 mm, as shown in Figure 10.

Looking the trajectory comparison (Figure 10(a)), without the assistance of the ADAS control, the tire is fully lifted, without the driver possibly governing the vehicle. When the logic is activated, Figure 10(b), braking the rear tires, the vehicle speed reduces down the critical hydroplaning one. Therefore, the vehicle gains drivability, helping the driver to avoid the cones.

Figure 11 highlights the torque vectoring action when the steering wheel angle asked by the driver is larger then $|5|$ degrees. In the first rows of cones (250m–290 m), the driver must perform a lane change on the left. Thus, a larger braking torque is applied on the rear left tire. Then the driver must steer on the right (290 m–310 m) to remain in the new lane, leading to a larger torque on the rear right tire. The driver remains on the lane for 30 m, where the steer is straight, and the vehicle speed is under the critical one; no torque vectoring is required. Finally, the driver comes back on the original lane (340 m–370 m). Once again, a larger torque is required on the rear left tire.

Driver in the loop simulation

Driver-in-the-loop (DIL) simulation bridges the gap between the real world and simulation. It is fundamental since human behavior during dangerous conditions can be considered. The testing activity has been carried out at DriSMi (Driving Simulator of the Politecnico di Milano), a laboratory that houses a new generation dynamic driving simulator (Gobbi et al., 2022).

This section analyzes the impact of activating the ADAS control system. An objective assessment is performed by comparing the vehicle trajectory in tests conducted with the control system both enabled and disabled. This analysis aims to quantify the effectiveness of the hydroplaning scenario generated using the novel tire model and to evaluate the performance of the proposed ADAS strategy when integrated with a human driver in a realistic and potentially hazardous scenario (Figure 12).

The experimental campaign involved a panel of 37 drivers to evaluate the efficacy of the control logic. The participants included 10 novice drivers, defined as having obtained their driving license within the last 3 years in accordance with Italian law, and 27 experienced drivers. Among the participants, 9 were female and 28 were male. Additionally, 7 participants reported having attended driving courses, while 18 had prior experience with hydroplaning. The effectiveness of the control logic was then assessed by the different rates of success in completing the maneuvers.

For both the maneuvers, a speed of 105 km/h and 5 mm puddle depth has been considered.

Figure 12. Driving simulator of the Politecnico di Milano (Gobbi et al., 2022).

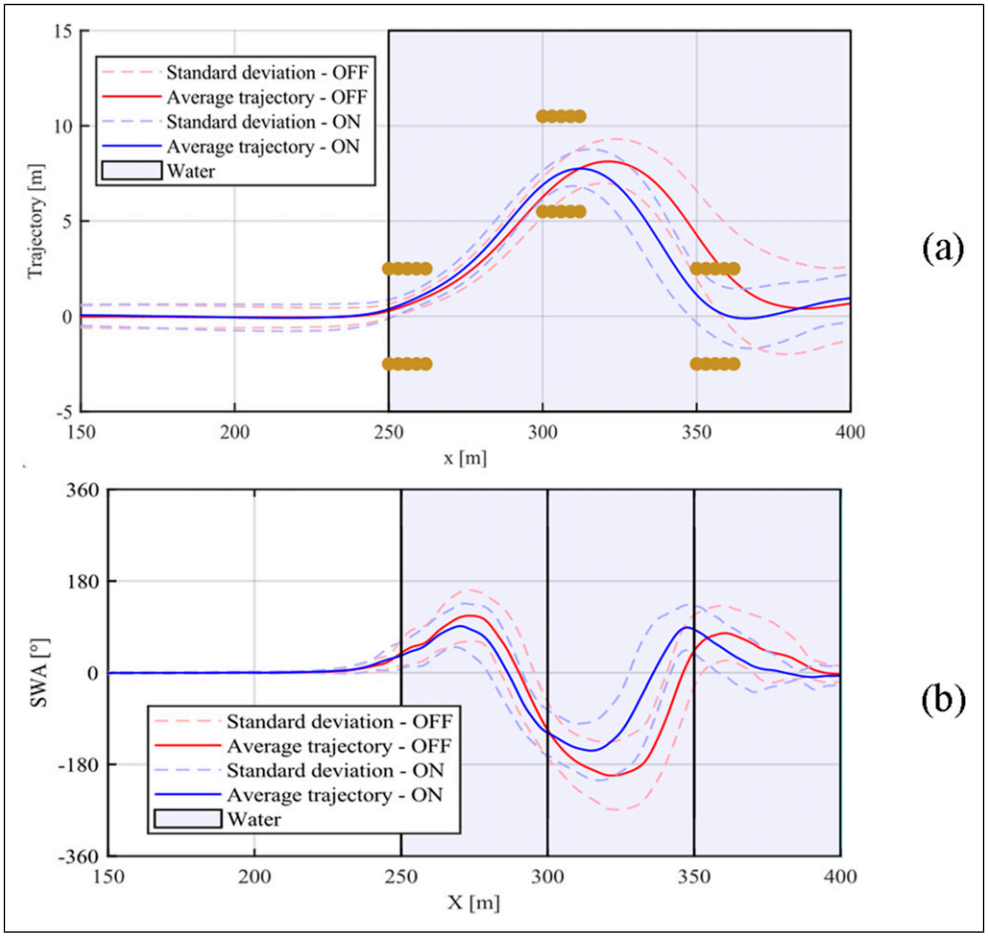

Figure 13. Average and standard deviation of the drivers with (blue) and without (red) ADAS assistance: trajectories (a), SWA (b).

Double lane change

The first maneuver result is reported in the next figures. With the assistance of the ADAS, drivers are able to avoid obstacles and complete the maneuver safely. Figure 13(a) highlights the standard deviation of the trajectory (dashed lines), and the average of the trajectories followed by the drivers (solid lines). Taking advantage of the ADAS logic, the drivers can close the maneuver without crashing into the cones (yellow dots). Indeed, the standard deviation of the trajectories is always within the rows of cones.

Figure 13(b) highlights the steering wheel angle required by the drivers. It is interesting that in the case of ADAS OFF, drivers are always late with respect to the cones. Thus, they are going to crash into them. Furthermore, to counteract the delay, they are asking for more steering wheel. To avoid crashing into the cones, it is therefore necessary higher skills.

Figure 14 highlights the lateral force exchanged with the ground by the tires. It is interesting to notice how the level of force exchanged by the front tires during the first lane change is larger when the logic is active. Therefore, the logic was able to reduce the vehicle speed under the critical hydroplaning one. Moreover, when the control logic is deactivated, the front tire forces exhibit a delay relative to the obstacle positions, impairing the driver's ability to effectively avoid them. This delay arises from the tire's relaxation length and cornering stiffness, which contribute to a lag in the build-up of lateral forces.

Finally, Figure 15 reports the evolution of the braking torque produced by the logic. In the first part, before 300 m, the vehicle must move on the left, so larger torque is applied to the left tire. Slightly before 300 m, drivers start moving again on the right to the original lane, thus larger torque is applied on the right. After 320 m, the vehicle's speed is below the critical hydroplaning one, thus the less torque is applied.

Constant radius high-speed turn

The second maneuver result (Figure 16(a)) is reported in the next figures. With the assistance of the ADAS, all drivers perform the turn and complete the maneuver safely. Without

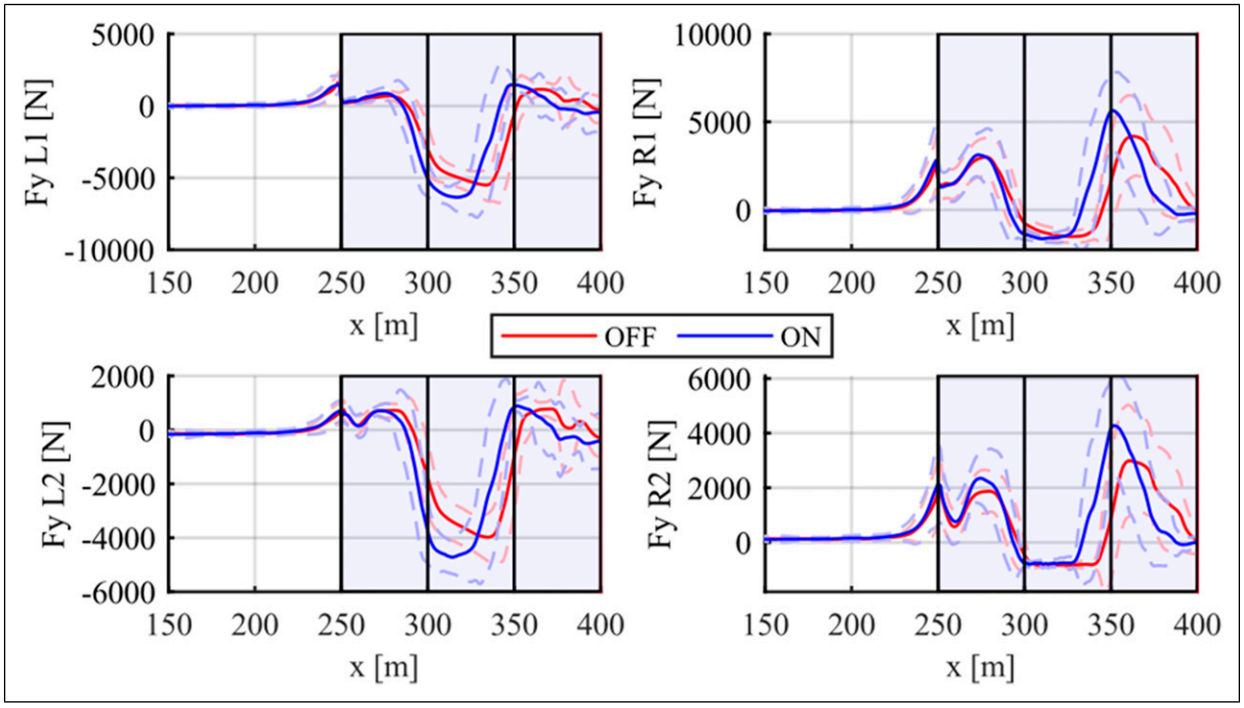

Figure 14. Average and dispersion of the lateral forces developed by the tire with (blue) and without (red) ADAS control logic during DLC.

the assistance of the ADAS, almost all drivers are unable to fulfill the maneuver. The average is out of the limits, and the variance is large.

Figure 16(b) highlights the steering wheel angle asked by the drivers. Without ADAS logic activated, drivers must ask for a larger steering angle to close the maneuver. The vehicle is always late concerning the turn, since the lateral force build-up is delayed due to relaxation length and cornering stiffness drop of performance.

Looking at the lateral forces on the tires, the reduction of the vehicle speed thanks to the ADAS helps in reaching the maximum force exchangeable with the

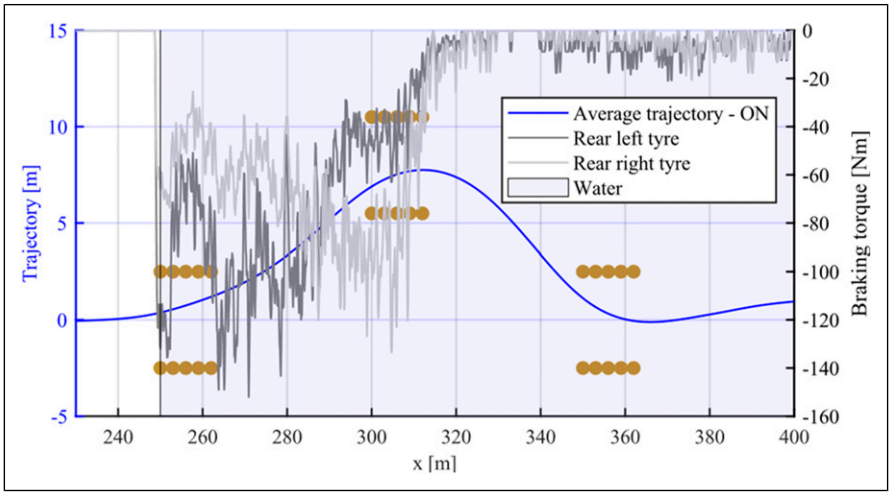

Figure 15. Average braking torque applied on rear tires with control logic active, during DLC.

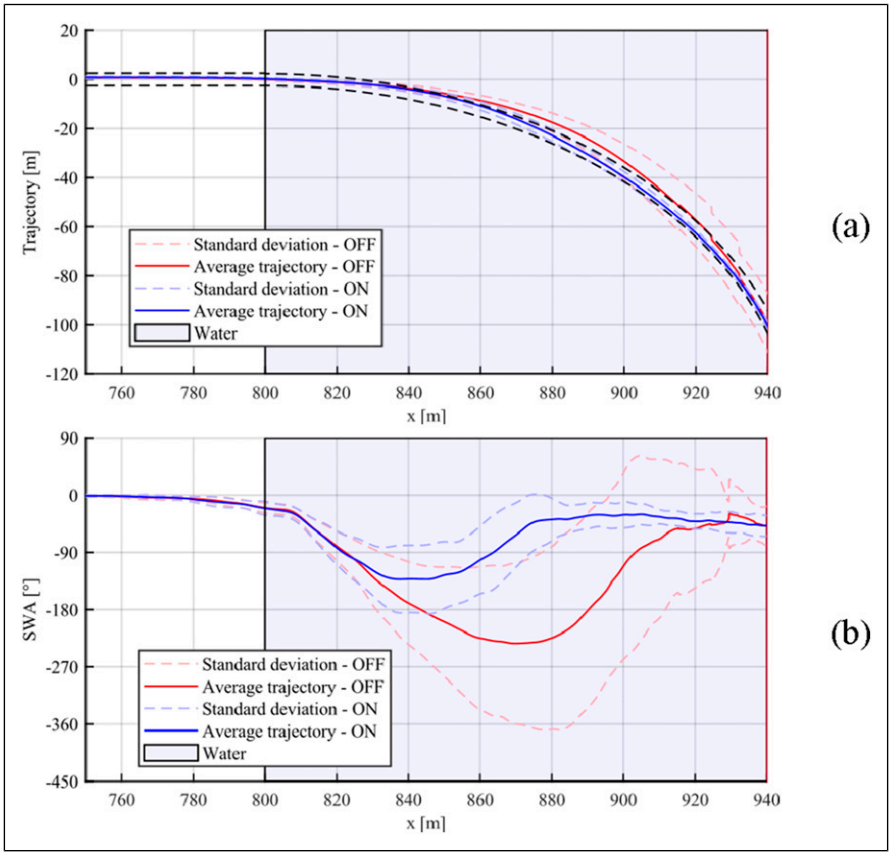

Figure 16. Average and standard deviation of the drivers with (blue) and without (red) ADAS assistance: trajectories (a), SWA (b).

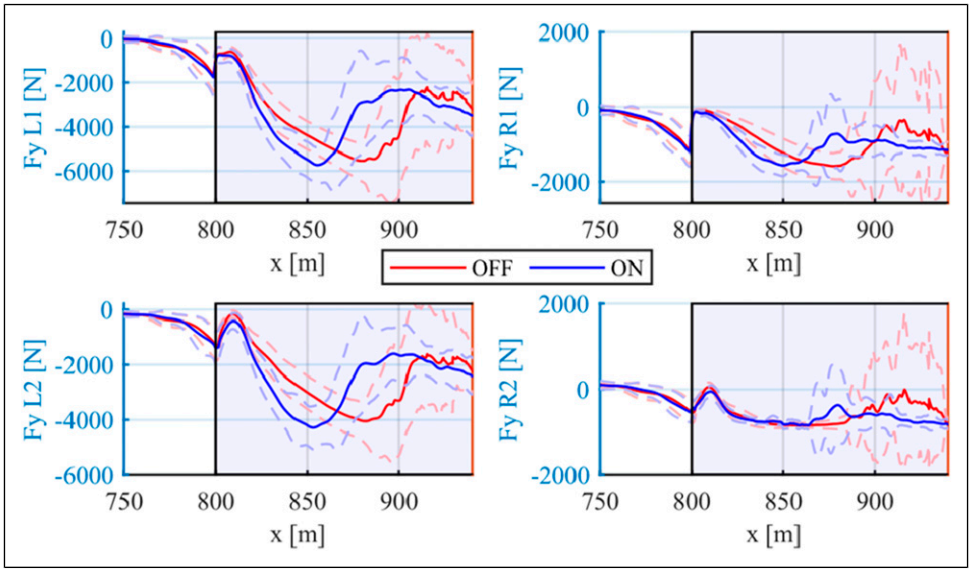

Figure 17. Average and dispersion of the lateral forces developed by the tire with (blue) and without (red) ADAS control logic during high-speed turn.

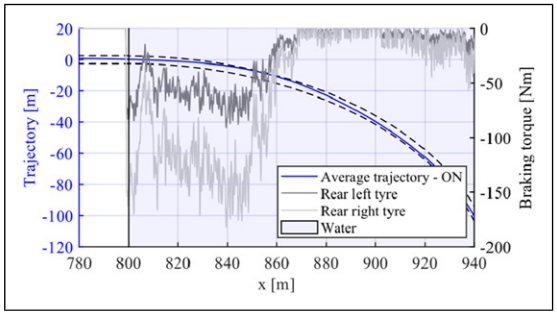

Figure 18. Average braking torque applied on rear tires with control logic active, during high-speed turn.

ground in a lower amount of time. Furthermore, since the drivers are steering on the right, the lateral load transfer increases the weight on the left tires (Figure 17).

Finally, it is possible to compare the torque applied on the rear axle (Figure 18). Since the turn is characterized by a constant radius, the rear right (inner) tire undergoes to larger lateral force. This torque vectoring helps the drivers in steering the vehicle.

Conclusion

This work introduces an Advanced Driver Assistance System (ADAS) designed to prevent or mitigate hydroplaning effects by leveraging smart tire technology. To enable the simulation of hydroplaning conditions and their assessment in a driving simulator, an enhanced tire model was developed. The model builds upon the traditional Magic Formula by integrating velocity-dependent scaling factors, further extended to account for the water depth, and additional physical phenomena relevant to wet conditions, such as the cleaning effect of rear tires. The model was compared with sine sweep test data available in the literature to verify its consistency and capability to reproduce key trends observed under hydroplaning scenarios, providing a solid basis for ADAS development.

Once the tyre model was ready and validated, a control system was designed to counteract the hydroplaning. The system working principle is a reduction of the vehicle speed well below the critical hydroplaning one. To activate it, it has been assumed to have smart tires on-board the vehicle itself.

An experimental testing campaign has been performed at the DriSMi laboratory, in Politecnico di Milano. Human drivers tested the control strategy, confirming its effectiveness in completing maneuvers that were otherwise impossible. Offline simulations and driver-in-the-loop driving simulator tests provided key insights into driver behavior and control strategy performance.

ORCID iDs

Edoardo Montini https://orcid.org/0009-0009-3593-590X
Stefano Melzi https://orcid.org/0000-0001-9138-6225

Funding

The authors received no financial support for the research, authorship, and/or publication of this article.

Declaration of conflicting interests

The authors declared no potential conflicts of interest with respect to the research, authorship, and/or publication of this article.

References

Aboeòsaoud M, Taha AA, Abo Elazm M, et al. (2025) A dynamic hydroplaning study: A fluid-structure interaction model for road vehicle tire analysis. *SAE International of Passenger Vechicle Systems* 18(3): 221–241. https://doi.org/10.4271/15-18-03-0015

Albert BJ (1968) *Tyres and hydroplaning, automotive engineering congress and exposition*. SAE International.

Arosio D, Braghin F, Cheli F, et al. (2005) Identification of Pacejka's scaling factors from full-scale experimental tests. *Vehicle System Dynamics* 43(1): 457–474. https://doi.org/10.1080/00423110500229683

Bielse F, Hermange C, Todoroff V, et al. (2022) Experimental investigation of the leading parameters influencing the hydroplaning phenomenon. *Vehicle System Dynamics* 60(11): 2375–2392.

Blandina GA and Fassio D, (2020). An active safety system able to counter acquaplaning, integrated with sensorized tires, adas and 5g technology for both human-driven and autonomous vehicles. In: *Conference on Sustainable Mobility*. SAE International, Sep 2020.

Braghin F, Cheli F and Sabbioni E (2006) Environmental effects on Pacejka's scaling factors. *Vehicle System Dynamics* 44(7): 547–568. https://doi.org/10.1080/00423110500520065

Cerezo V, Gothie M, Menissier M, et al. (2010) Hydroplaning speed and infrastructure characteristics. *Proceedings of the Institution of Mechanical Engineers - Part J: Journal of Engineering Tribology* 224(9): 891–898. https://doi.org/10.1243/13506501jet738

Erseus A, Trigell AS and Drugge L (2013) Methodology for finding parameters related to path tracking skill applied on a DLC test in a moving base driving simulator. *International Journal of Vehicle Autonomous Systems* 11(1): 1–21.

Fichtinger A, Edelmann J, Plochl M, et al. (2021) Aquaplaning detection using effect-based methods: an approach based on a minimal set of sensors, electronic stability control, and drive torques. *IEEE Vehicular Technology Magazine* 16(3): 20–28. https://doi.org/10.1109/mvt.2021.3085536

Fwa T, Srirangem S, Anupam K, et al. (2009) Effectiveness of tyre-tread patterns in reducing the risk of hydroplaning.

Transportation Research Record Journal of the Transportation Research Board 2094: 91–102.

Gobbi M, Mastinu G, Melzi S, et al. (2022) A driving simulator for UN157 homologation activities. In: Proc. of the ASME International Design Engineering Technical Conferences and Computers and Information in Engineering Conference, Houston, TX, USA, 23–26 August 2026.

Hartman B and Raste T (2019) *Hydroplaning Avoidance – a Holistic System Approach*. Klöster.

Jalali K, Uchida T, McPhee J, et al. (2013) Development of an advanced fuzzy active steering controller and a novel method to tune the fuzzy controller. *SAE International Journal of Passenger Cars – Electronic and Electrical Systems* 6(1): 241–254.

Jindřich F, Motl J, Mikulec R, et al. (2019) Acquaplaning-preventing device based on blowing a wet road with a stream of air. *Transportation Research Proceding* 44(Suppl 1): 290–296.

Kienle R, Ressel W, Götz T, et al. (2020) The influence of road surface texture on the skid resistance under wet conditions. *Proceedings of the Institution of Mechanical Engineers* 234(3): 313–319.

Malenska M, Petry F, Fehr D, et al. (2021) Longitudinal hydroplaning performance of passenger car tyres. *Vehicle System Dynamics* 59(11): 1–18.

Metz LD (2011) Hydroplaning behaviour during steady-state cornering maneuvers. *SAE Internation Journal of Materials and Manufacturing* 4(1): 1068–1079.

Metz LD (2012) *Potential for hydroplaning behavior during transient maneuvers*. SAE Int.

Metz LD (2014) Simulation of transient maneuver hydroplaning events using HVE. *SAE Technical Paper 2014-01- 0122,* 1: 2014. https://doi.org/10.4271/2014-01-0122

Metz LD, Kinney JR and Herling D (2006) *Realistic rear axle hydroplaning during forward motion*. SAE Int.

Mounce JM and Bartoskewitz RT (1993) *Hydroplaning and roadway tost 10.1016/j.triboint.2025.111579liability.* Transportation Research Record.

Mueller J, Stanley S, Martin T, et al. (2014) Driving simulator and scenario effects on driver response. In: Proceedings of the 2014 Industrial and Systems Engineering Research Conference, Canada, 31 May–3 June 2014.

Niskanen AJ and Tuononen AJ (2014) Three 3-axis accelerometers fixed inside the tyre for studying contact patch deformations in wet conditions. *Vehicle System Dynamics* 52(Suppl 1): 287–298.

Niskanen AJ and Tuononen AJ (2015) Accelerometer tyre to estimate the aquaplaning state of the tyre-road contact. In: IEEE Intelligent Vehicles Symposium IV, Seoul, Korea, 28 June–01 July 2015.

Pacejka HB, (2006). Tyre and vehicle dynamics. In: *Butterworth-Heinemann, Chapter 4: "Semi-Empirical Tyre Models"*, (pag 176-182).

Raste T and Frerichs (2016) *Study on Active Safety for Acquaplaning Assistance*, Advanced Vehicle Control.

Sbrosi M, D'Alessandro V, Melzi S, et al. (2012) Phenomenological analysis of hydroplaning through intelligent tyres. *Vehicle System Dynamics* 50(Suppl 1): 3–18.

Wong J (2001) *Theory of Ground Vehicles*. Wiley.

World Health Organization (2019) *Global Status Report on Road Safety.*

Yu Y, Wang H, Wu Y, et al. (2026) Skid resistance assessment of wet asphalt runways by coupling finite element simulation with real texture evolution data. *Tribology International* 216: 111579. https://doi.org/10.1016/j.triboint.2025.111579

Zhong Q, Wang Y, Zhou X, et al. (2025) Simulation analysis of tire viscous hydroplaning on wet pavement. *Proceedings of SPIE - The International Society for Optical Engineering* 13781, art. no. 1378107: 193. Available at: https://doi.org/10.1117/12.3079170